



# Faraday Discussions

## Surface polarization enhances ionic transport and correlations in electrolyte solutions nanoconfined by conductors

Journal:	<i>Faraday Discussions</i>
Manuscript ID	FD-ART-02-2023-000028.R1
Article Type:	Paper
Date Submitted by the Author:	10-Mar-2023
Complete List of Authors:	Jimenez-Angeles, Felipe; Northwestern University, Materials Science and Engineering Ehlen, Ali; Northwestern University, Applied Physics Program Olvera de la Cruz, Monica; Northwestern University, Materials Science and Engineering

SCHOLARONE™  
Manuscripts

## ARTICLE

## Surface polarization enhances ionic transport and correlations in electrolyte solutions nanoconfined by conductors

Felipe Jiménez-Ángeles<sup>a,†</sup>, Ali Ehlen<sup>b</sup>, and Monica Olvera de la Cruz<sup>a,b,c</sup>

Received 00th January 20xx,  
Accepted 00th January 20xx

DOI: 10.1039/x0xx00000x

Layered materials that perform mixed electron and ion transport are promising for energy harvesting, water desalination, and bioinspired functionalities. These functionalities depend on the interaction between ionic and electronic charges on the surface of materials. Here we investigate ion transport by an external electric field in an electrolyte solution confined in slit-like channels formed by two surfaces separated by distances that fit only a few water layers. We study different electrolyte solutions containing monovalent, divalent, and trivalent cations, and we consider walls made of non-polarizable surfaces and conductors. We show that considering the surface polarization of the confining surfaces can result in a significant increase in ionic conduction. The ionic conductivity is increased because the conductors' screening of electrostatic interactions enhances ionic correlations, leading to faster collective transport within the slit. While important, the change of water's dielectric constant in confinement is not enough to explain the enhancement of ion transport in polarizable slit-like channels.

### Introduction

Ions transport in strongly confined fluids plays a key role in biological processes and nanoscale applications, including ion exchange between cells and their surrounding aqueous medium, nanofluidic energy conversion, and water desalination.<sup>1-3</sup> Slit-like pores fabricated of layered materials allow studying thin liquid films of thicknesses down to the nanometre scale,<sup>4</sup> leading to the discovery of new properties of water and ions, such as the suppression of the dielectric permittivity in water films consisting of two or three molecular layers,<sup>5</sup> and room-temperature phase transitions.<sup>6-8</sup> Studies of ion transport in slit-like channels show that an applied voltage acts as a gate of a pressure-driven current.<sup>9</sup> Interestingly, in that work, slit-like channels of graphite and hexagonal boron nitride (hBN) exhibit marked differences in the ion transport attributed solely to the properties of the confining surfaces. Specifically, hBN is an insulator, whereas graphite has properties of dielectrics and conductors due to its anisotropy.<sup>10</sup> In the basal plane's normal direction, the electric conductivity is at least four orders of magnitude lower than along the directions of the basal plane. As a consequence, while graphite conducts in-plane, a

dielectric constant in the basal plane's normal direction can be measured in graphitic materials, and its value is similar to that of hBN.<sup>11-12</sup>

The phenomena described in the previous paragraph underscore the need to consider the coupling between the electrons on a surface interacting with atoms and molecules from another material. The coupling between the electronic and atomic interactions occurs because atomic charges induce interfacial polarization charges on nearby surfaces. To consider the surface polarization charges induced by charges near interfaces, it is necessary to impose distinct electrostatic boundary conditions on dielectrics and conductors. In conductors, the surface electrostatic potential is maintained constant,<sup>13-14</sup> whereas dielectrics require the continuity of the displacement field.<sup>15-16</sup> The image charge method is employed to solve the electrostatic boundary condition equations,<sup>17-19</sup> but it is difficult to extend to non-planar interfaces and can be computationally expensive. The fluctuating charges methods<sup>14, 20-22</sup> consist of adjusting the surface polarization charges on-the-fly to minimize the electrostatic energy. A recent method employs periodic Green functions to consider the surface polarization.<sup>23</sup> Atomistic models consider the atomic polarizability in dielectrics using the Drude model of fluctuating induced dipoles.<sup>24</sup> However, this approach is not extensible to conductors.

The metallic nature of conductors leads to different degrees of electronic screening.<sup>25</sup> The Thomas-Fermi (TF) model is suggested to explain the degree of electronic screening in non-perfect conductors.<sup>26</sup> In the TF model, the charges in a solid are

<sup>a</sup> Department of Materials Science and Engineering, Northwestern University, Evanston, Illinois 60208, USA

<sup>b</sup> Applied Physics Program, Northwestern University, Evanston, Illinois 60208, USA

<sup>c</sup> Department of Physics, Northwestern University, Evanston, Illinois 60208, USA

† e-mail: felipe.angeles@northwestern.edu

Electronic Supporting Information (ESI) available: Complementary simulation details, results from gated and ungated electrodes, derivation of an analytical expression of the force between two ions confined by conductors. See DOI: 10.1039/x0xx00000x

envisioned as an electron gas in a neutralizing background. The quantum effects are considered using a finite screening length  $\lambda_{TF}$  of the interactions between polarization charges. The TF theory<sup>27</sup> considers that the charge density in an electron gas is approximated by  $q_{TF}\rho^P(\mathbf{r}) = -\varepsilon_0\varepsilon_r k_{TF}^2 \psi_B(\mathbf{r})$ , similar to the Debye-Hückel theory for electrolytes;  $\varepsilon_0$  is the vacuum permittivity,  $\varepsilon_r$  is the dielectric constant of the medium,  $k_{TF} = \lambda_{TF}^{-1}$  is the inverse screening length, and  $\psi_B(\mathbf{r})$  is the electrostatic potential in the conductor. In perfect conductors  $\lambda_{TF}^{-1} \rightarrow \infty$ . The TF approximation, however, is only valid in the limit of infinite nuclear charge.<sup>28</sup>

The electronic screening affects the properties of a nearby ionic fluid. To consider the electronic screening of conductors next to an ionic fluid, a TF fluid is considered as an ionic mixture within a region of width  $d_{TF}$  inside the conductor.<sup>26</sup> It is found that the screening from the TF fluid shifts the wetting and phase transition points of confined ionic liquids.

Water and ions in confinement play a key role in numerous applications. Therefore, it is of paramount importance to understand how water and electrolyte solutions are affected by the properties of the confining materials. Recently, we showed that the water polarization near an interface breaks the symmetry of electrostatic interactions.<sup>29</sup> The symmetry breaking implies that the potential of mean force between two oppositely charged ions near a liquid-solid interface, interacting along the interface's normal direction, differs by  $5 k_B T$  when exchanging the ions' position with respect to the surface. Here, we use molecular dynamics simulations to investigate ionic transport in aqueous solutions confined in slit-like-channels formed by conductors. To account for the interaction between conductive surfaces, ions, and water, we assign fluctuating polarization charge on the atoms of the conductors with a spatial Gaussian distribution<sup>13-14</sup>. We propose using the width of the Gaussian distributions  $\kappa^{-1}$  to model the electronic screening in non-perfect conductors.

## Methods

### Molecular Dynamics

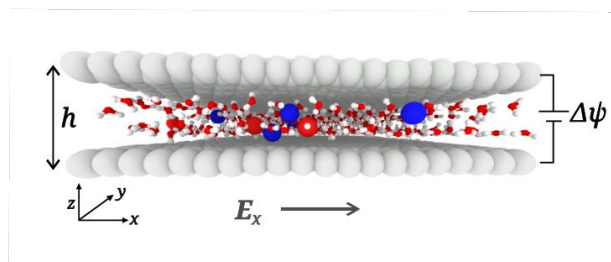


**Figure 1:** Simulation setup consisting of an electrolyte solution confined by a slit-like channel formed by two surfaces with separation distance  $h$  measured from the carbon atoms' center. The particles size is reduced in this image to visualize the ions. Polarizable surfaces of conductors are maintained at constant potentials  $\psi_t$  and  $\psi_b$  at the top and bottom electrodes, respectively. The potential difference is  $\Delta\psi = \psi_t - \psi_b$ . Non-polarizable surfaces are assigned constant surface charge densities,  $\sigma_t$  and  $\sigma_b$  at the top and bottom electrodes, respectively. An external electric field  $E_x$  is applied in parallel surfaces' direction to induce the ions' transport.

We consider an ion solution consisting of  $N_w$  water molecules,  $N_+$  cations, and  $N_-$  anions confined between two surfaces modelled using graphene sheets. The surfaces are parallelly placed on the x-y plane separated by a distance  $h$  in the z-direction (see Figure 1). We use graphene sheets made of 1008 carbon atoms each. The system is placed in a simulation box of dimensions  $L_x = 5.065$  nm and  $L_y = 5.104$  nm, in the x- and y-directions, respectively. The box length in the z-direction is  $L_z \gg h$ . To mimic two-dimensional (2D) periodicity in the x- and y-directions, we use the slab correction<sup>30</sup> in three-dimensional boundary conditions (3DC). We set  $h = 0.97$  nm to study the dielectric response of water and an electrolyte solution. The water layer is made of 580 water molecules. The electrolyte solution is made of 560 water molecules, 10 cations, and 10 anions. Water is represented using the extended simple point charge<sup>31</sup> (SPC/E) model, and the AA-OPLS force field parameters are employed to represent the van der Waals interactions of graphene and the ions.<sup>32</sup>

We study the systems when the surfaces are conductors and non-polarizable. In conductors, the surface potential at the top and bottom surfaces (see Figure 1) is kept constant at  $\psi_t$  and  $\psi_b$ , respectively, and the potential difference is  $\Delta\psi = \psi_t - \psi_b$ . In non-polarizable electrodes, the surface charge density at the top and bottom surfaces are constant at  $\sigma_t$  and  $\sigma_b$ , respectively. We study the cases when the surfaces are at zero charge and zero surface potential and are asymmetrically charged. In general, the potentials in conductors are assigned as  $\psi \equiv \psi_t = -\psi_b$ , whereas in the non-polarizable surfaces, the charges are assigned as  $\sigma \equiv \sigma_t = -\sigma_b$ . The system formed by conductors are referred to as constant potential systems ( $\psi$ ), whereas the non-polarizable systems are referred to as constant charge density ( $\sigma$ ) systems. In the constant charge systems, each atom on the bottom and top electrodes has a charge  $q_b$  and  $q_t$ , respectively. The charges are assigned using the average simulation values at a constant potential. In the next section, we outline the method to maintain a constant potential on the surfaces.

To induce the ionic transport, the external electric field is applied tangentially to the surface in the x-direction and designated as  $E_x$ . The force due to the external field on each charged atom or ion is  $\mathbf{f}_i = q_i \mathbf{E}_x$ . The magnitude of the effective field experienced by any charge in the system  $|\mathbf{E}|$  is smaller than  $|\mathbf{E}_x|$  due to the polarization of water and other charged particles in the system in response to  $E_x$ . Later, we discuss the implications of polarization in water and how our results could be related to experimental measurements.

The ions' equations of motion are integrated using the standard molecular dynamics algorithms implemented in LAMMPS.<sup>33</sup> The system temperature is maintained at  $T = 298$  K. We compared the cases when the slit surfaces are made of conductors and non-polarizable materials.

### Constant Potential

We use the model introduced by Siepmann and Sprik<sup>13-14</sup> that consists in assigning a Gaussian distribution of the polarization charge on each of the electrode's atoms

$$\rho_P(\mathbf{r}) = \sum_{i=1}^{N_e} q_i \left( \frac{\kappa^2}{\pi} \right)^{\frac{3}{2}} e^{-\kappa^2(\mathbf{r}-\mathbf{R}_i)^2} \quad (1)$$

where  $\kappa$  is the inverse width of the distribution centered at the position  $\mathbf{R}_i$  of each one of the  $N_e$  atoms forming the electrodes. The charge of the water atoms and the ions is considered using a Dirac delta function for each atomic position  $\mathbf{r}_i$  containing a point charge

$$\rho_F(\mathbf{r}) = \sum_i q_i \delta(\mathbf{r} - \mathbf{r}_i) \quad (2)$$

where the summation is performed over the charges of the atoms in the liquid. The electrostatic energy of the system is expressed as

$$U_C = \frac{1}{8\pi\epsilon_0} \iint \frac{\rho(\mathbf{r}')\rho(\mathbf{r}'')}{|\mathbf{r}'' - \mathbf{r}'|} d\mathbf{r}' d\mathbf{r}'' \quad (3)$$

where  $\rho(\mathbf{r})$  is the total charge density including the polarization charges of the electrode, and the charges from water molecules, and ions. The potential  $\psi_j$  on a charge  $q_i$  is obtained by taking the derivative of  $U_C$  with respect to this charge, keeping all the other charges constant

$$\psi_j = \left( \frac{dU_C}{dq_j} \right)_{q_i, i \neq j} \quad (4)$$

The charge of each electrode atom is obtained by imposing the potential constant on each atom,  $\psi_j = V_{0j}$ . This condition is achieved minimizing the constrained electrostatic energy function

$$U_E = U_C(q_i) - \sum_j \psi_j q_j \quad (5)$$

where the summation is performed over the charges of the electrodes. By writing the charge density as  $\rho(\mathbf{r}) = \rho_F(\mathbf{r}) + \rho_P(\mathbf{r})$ , where  $\rho_F(\mathbf{r})$  includes the charges in the fluid and  $\rho_P(\mathbf{r})$  includes the polarization charges in the electrode. Employing this definition, Eq. (3) is cast as

$$U_C = U_{FF} + U_{FP} + U_{PP} \quad (6)$$

where  $U_{FF}$  is the Coulombic interaction between the charges in the liquid,  $U_{FP}$  is the interaction between the liquid and the polarization charges, and  $U_{PP}$  is the interaction between the polarization charges. Setting the derivative of  $U_E$  equal to zero, and using Eq. 6, the potential on each atom of the electrode can be written as

$$\psi_j = \sum_k A_{jk} q_k + b_j \quad (7)$$

$A_{jk}$  includes the interaction terms of all the charges  $q_k$  on the electrode with the site  $j$ , whereas  $b_j$  includes the interaction term of the fluid particles with the site  $j$ . Because the positions of the electrode charged sites remain fixed in the simulation, the components of the matrix  $A_{jk}$  remain constant during the simulation, while the components of  $b_j$  are updated at each time step. Using matrix notation, the solution of Eq. (7) is written as

$$\mathbf{q} = \mathbf{A}^{-1}(\boldsymbol{\Psi} - \mathbf{b}) \quad (8)$$

where  $\mathbf{q}$  is a vector that contains the charges of the electrodes, and  $\boldsymbol{\Psi}$  contains the potential at the electrodes' charged sites. The computation of the polarization charges at each time step is necessary to perform molecular dynamics simulations. By using a Gaussian distribution the calculation of the electrostatic energy is performed using the available P3M algorithm to calculate long-range electrostatic interactions.<sup>21</sup> In our study  $\kappa = 18 \text{ nm}^{-1}$ .

## Results

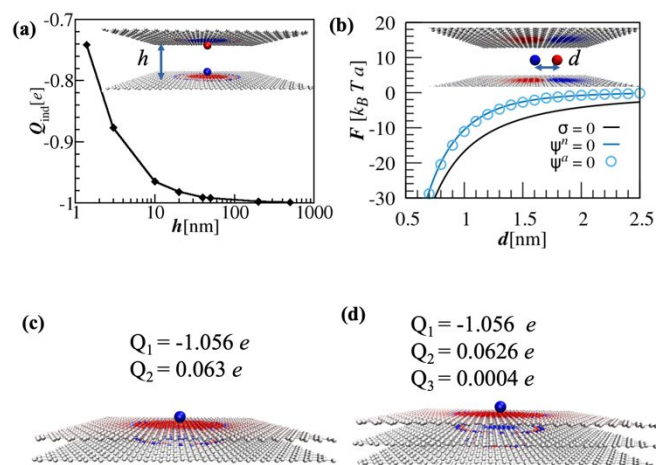


**Figure 2:** Polarization of conductive materials maintained at  $\psi_t = \psi_b = \psi = 0$ . (a) Induced polarization charge  $Q_{\text{ind}}$  on the conductor as a function of the surface-surface separation distance  $h$  when an ion is placed at 0.3 nm from each surface. The inset shows the ions' configuration between the two surfaces. Blue and red colors on the surface of conductors are assigned based on the magnitude and sign of the polarization charge; positive charges are colored in blue, and negative charges are in red. (b) Interaction force between a monovalent cation and a monovalent anion placed at the middle plane between the two conductors separated by a distance of  $h = 1.3 \text{ nm}$ ; the black line is calculated by neglecting the surface polarization ( $\sigma = 0$ ); the light blue line ( $\psi'' = 0$ ) is the force that includes the contributions from the polarization charges obtained by numerically solving Equation (8). The open circles represent ( $\psi'' = 0$ ) the force calculated

using the analytical image charge method (see Supporting Information). Polarization charges (showing only the bottom electrode) in slit-like channels formed surfaces of (c) two and (d) three layers. The surfaces' separation distance is  $h = 50$  nm. The induced charges  $Q_1$ ,  $Q_2$ , and  $Q_3$  are numbered from the closest layer to the ion.

First, we study the polarization charge induced by ions located at the center of the simulation box in the  $x$  and  $y$  directions and  $0.3$  nm from the conductors separated by  $h$  (See inset of Figure 2a). It is well known in electrostatics that near the surface of single conductor, an ion of charge  $q$  induces an image charge of the same magnitude as its own but of the opposite sign  $-q$ . However, when an ion is confined by two conductors, the polarization charge is induced on both conductors and depends on the surfaces' separation distance and the ion's position with respect to the surfaces. We consider the configuration in the inset of Figure 2a that contains two oppositely charged ions placed symmetrically at  $(L_x/2, L_y/2, \pm(h/2 - 0.3\text{nm}))$ . We see that the magnitude of the total induced charge on a given conductor is lowered by the presence of the other parallel conducting surface. In this configuration, the magnitude of the induced charge on the conductor is equal to that of the nearby ion only when the separation  $h$  is in the range of  $1000$  nm.

We now investigate how the interaction between two ions is changed by the presence of the two surfaces. For that, we calculate the interaction force between two oppositely charged ions placed at the middle plane between the two surfaces separated by  $h = 1.3$  nm. Figure 2b shows the interaction forces between the two ions confined between polarizable and unpolarizable surfaces as a function of their separation distance  $d$  (see inset of Figure 2b). We observe that the magnitude and range of the attraction are reduced between ions confined by conductors with respect to the interaction between non-polarizable surfaces. The reduction is caused by the polarization charges on the conductors that screen the interaction between the confined charges.

Now we investigate the induced surface charge in multi-layered surfaces separated by  $h = 50$  nm. In single-layered conductors at  $h = 50$  nm, the absolute value of the induced charge  $|Q_{\text{ind}}|$  is approximately  $0.992e$ . In multi-layered conductors, the polarization charge is induced as far as three layers from the closest surface to the ion. We find that the absolute value of the induced charges on the closest layer to the ion  $Q_1$  is larger than  $1e$ , while a charge of the opposite sign is induced on the second layer  $Q_2$ . The induced charge in the third layer is negligible and is similar in surfaces made of three or more layers. The overall charge in single-layer and multi-layer conductors is similar. However, the polarization is distributed differently depending on the number of layers. Our results imply that the induced charge fluctuations on single-layered materials are affected by the induced polarization of a supporting substrate.<sup>34</sup>

### Static properties of confined water and ions

Given that the presence of conductors impacts charged interactions, we are interested in how this effects a more realistic system. We investigate the behavior of a water layer confined between two surfaces separated by  $h = 0.97$  nm. The polarization charge on the conductors is induced by the charges of oxygen and hydrogen atoms from water. Oxygen is negatively charged and induces positive polarization charges, whereas hydrogen bears a positive charge and induces negative polarization charges. In Figure 3a, we observe that the polarization charge on the conductors is distributed in a non-uniform way due to different conformations of the water molecules. Therefore, the total charge density  $\sigma$  on the surface of conductors is

not constant. Figure 3b shows the probability distribution of the induced charge densities on the surfaces at  $\psi = 0$  and  $0.5$  V. Figure 3b shows the results of water with no ions. We observe that the charge density fluctuates around a mean value  $\sigma_V$  that depends on the potential. We find that  $\sigma_V = 0.00$  and  $0.187$  e/nm<sup>2</sup> for potentials of  $\psi = 0$  and  $0.5$  V, respectively. By plotting the distribution around the mean value  $\sigma_V$ , the two curves overlap. An applied electric field in the surface parallel direction slightly changes the value of  $\sigma_V$  and the presence of different ion type too (see Figure S2 in the Supporting Information). The distribution width remains unchanged by the presence of ions, gating potential, and an applied electric field in the surface parallel direction (see Figure S2 in the Supporting Information). Therefore, while the mean value of the surface charge density changes with the potential, the width of the distribution is independent of the applied potential. This indicates that the fluctuations of the polarizations are regulated by the thermal fluctuations of the water molecules.

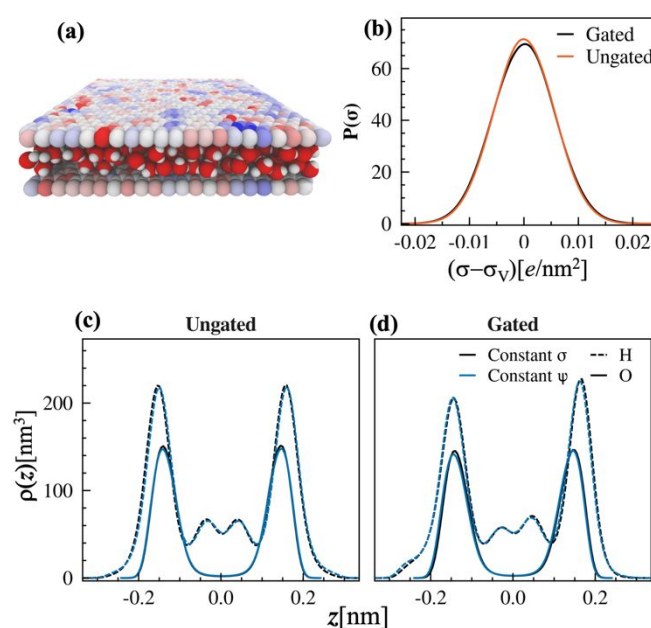


**Figure 3:** Effect of the surface polarization on confined water. (a) Snapshot of an instantaneous configuration of water confined between two conductive surfaces separated by  $h = 0.97$  nm. The surface atoms are colored by their charge; blue and red represent positive and negative charges, respectively; the intensity represents the magnitude. (b) Probability distribution  $P(\sigma)$  of the induced charge density  $\sigma$  plotted around the mean value  $\sigma_V$  that depends on the potential difference between the two surfaces. Density profiles  $\rho(z)$  of hydrogen and oxygen atoms from water between (c) uncharged non-polarizable ( $\sigma = 0$ ) and conductive ( $\psi = 0$ ) surfaces, and (d) charged non-polarizable ( $\sigma = 0.187$  e/nm<sup>2</sup>) and conductive ( $\psi = 0.5$  V) surfaces. The solid lines are the water oxygen atoms profiles, while the dashed lines are water hydrogen atoms profiles. The black lines represent the profiles in slit-like channels of conductors, while the light-blue lines are in non-polarizable surfaces. The  $z$ -coordinate is defined with respect to the middle plane between the two surfaces.

The hydrogen and oxygen density profiles are symmetric when the surfaces are ungated (see Figure 3c). When the surfaces are gated, the water molecules orient, and the negative surface preferentially adsorbs hydrogen atoms (see Figure 3d). Due to the water dipole moment and high density, the polarization effects from the surface are highly screened. Therefore, the hydrogen and oxygen density

profiles are not significantly different when the surfaces are conductors or non-polarizable. However, the dielectric responses and the ions' transport are affected by surface polarization, as we will see next.

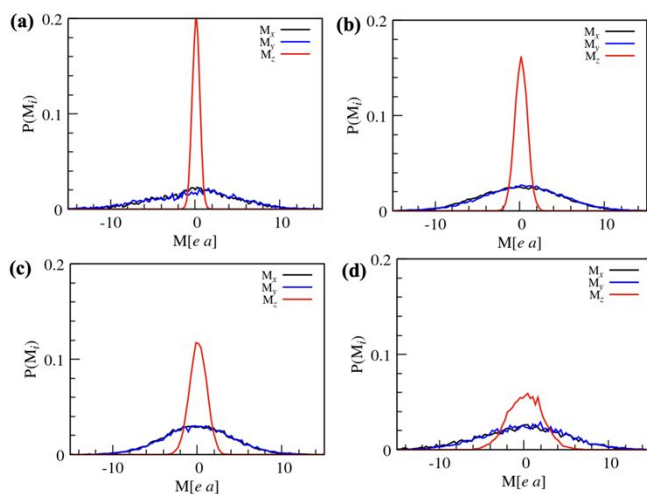


Figure 4 Dielectric response of confined water and an electrolyte solution. Probability distribution of the total dipole moment components  $M_i$ ,  $i = x, y, z$  of water between two (a) non-polarizable and (b) polarizable surfaces, and an electrolyte solution between (c) non-polarizable and (d) polarizable surfaces. The surfaces' separation is  $h = 0.97$  nm.

We investigate the changes in the dielectric response of water and an electrolyte solution confined by conductors and non-polarizable surfaces. We analyse our results in terms of polarization and the effective dielectric constant. The instantaneous polarization is calculated as  $\mathbf{p} = \frac{\mathbf{M}}{V}$ , where  $\mathbf{M} = \sum_{i=1}^{N_w} \mathbf{\mu}_i$  is the dipole moment ( $\mathbf{\mu}_i$ ) including all the water molecules in the volume  $V$ . The components of the dielectric tensor are given as<sup>35-36</sup>

$$\epsilon_{\parallel} = 1 + \left( \frac{\beta}{2\epsilon_0} \right) [\langle \mathbf{M}_{\parallel}^2 \rangle - \langle \mathbf{M}_{\parallel} \rangle^2] \quad (9)$$

$$\epsilon_{\perp}^{-1} = 1 - \left( \frac{\beta}{\epsilon_0} \right) [\langle \mathbf{M}_{\perp}^2 \rangle - \langle \mathbf{M}_{\perp} \rangle^2] \quad (10)$$

Where subscripts  $\parallel$  and  $\perp$  designate the components in the parallel and perpendicular directions of the slit pore surfaces, respectively;  $\epsilon_0$  is the vacuum permittivity,  $\beta = 1/(k_B T)$ ,  $k_B$  is the Boltzmann constant, and  $T$  is the absolute temperature. The dielectric constant in the parallel direction is proportional to the dipole moment fluctuations (see Eq. 9) whereas the component in the perpendicular direction is inversely proportional to the dipole fluctuations (see Eq. 10).

We analyze the dipole moment fluctuations of water and an electrolyte solution confined in a slit-like pore of  $h = 0.97$  nm. Figure 4a shows the probability distribution of the total dipole moment components of water. In the  $z$ -direction, the distribution is much narrower than in the  $x$ - and  $y$ -directions in agreement with the results from the literature.<sup>29, 37</sup> When water is confined by conductors (see Figure 4b), the dipole moment

probability distributions become broader, and their height decreases with respect to the non-polarizable surfaces in 4a. The ions have a similar effect as the conductive surfaces by reducing the height and increasing the width of the dipole moment probability distributions (see Figure 4c). By placing the electrolyte solution between conductors, the water dipole moment further decreases. The fluctuating total dipole moment of the liquid synchronizes with the induced polarization charge on the surfaces so that the total dipole moment of the system (liquid and polarizable surfaces) is *always* zero.

From the dipole moment fluctuations we obtain the dielectric constant of water using Equations 9 and 10. The parallel dielectric constant of water confined by non-polarizable surfaces ( $\sigma = 0$ ) is about  $\epsilon_{\parallel} \approx 94.5$ . This value is higher than the reported value in bulk for the SPC/E water model. By confining the water between conductive surfaces ( $\psi = 0$ ), the parallel dielectric constant is about 82. In the presence of ions  $\epsilon_{\parallel}$  is around 60 when the solution is confined by conductors ( $\psi$ ) or non-polarizable surfaces ( $\sigma$ ). In non-polarizable surfaces, the perpendicular dielectric constant is about  $\epsilon_{\perp} \approx 3.5$ , which agrees with the measured dielectric constant of water in high confinement<sup>5</sup>. When water is confined by conductors and in the presence of ions, Eq. 10 leads to negative values of  $\epsilon_{\perp}^{-1}$ . This analysis shows that the perpendicular dielectric constant of confined water is significantly lower than in bulk, but in the surfaces' parallel direction can be higher than in bulk. In ultra-thin water layers, the ion-ion interactions mostly occur in the surfaces' parallel direction. Therefore, the interactions are significantly diminished due to the high parallel dielectric constant.

### Ion transport in confinement

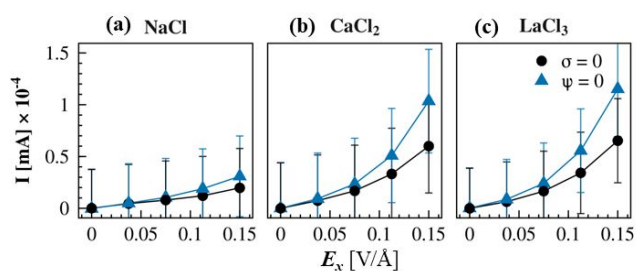
We investigate ionic transport in the slit channel described in Figure 1. To induce the ion transport, we apply an electric field tangentially to the channel surfaces in the  $x$ -direction,  $E_x$ . The ion current is given as

$$I = \left\langle \sum_{i=1}^{N_i} \frac{q_i v_i}{L_x} \right\rangle_{\tau} \quad (11)$$

$N_i$  is the number of free charges (ions) in the system,  $q_i$  is the ionic charge,  $v_i$  is the instantaneous ion velocity, and  $L_x$  is the simulation box size in the  $x$ -direction.  $\langle \rangle_{\tau}$  means that the average is calculated over the duration time of the simulation,  $\tau$ . We study the three electrolytes NaCl, CaCl<sub>2</sub>, and LaCl<sub>3</sub>. The ions' parameters are taken from the AA-OPLS force-field.<sup>32</sup> The compositions of the systems are given in Table S1 in the Supporting Information. We systematically compare the ionic transport in a channel formed by polarizable (conductors) and non-polarizable surfaces.

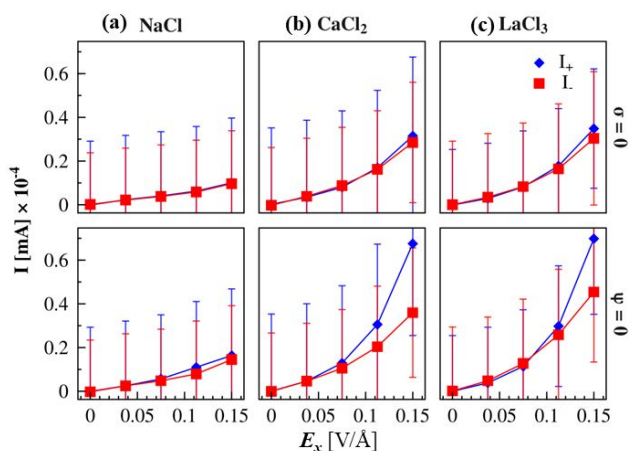
Figure 5 shows the current of NaCl, CaCl<sub>2</sub>, and LaCl<sub>3</sub> electrolyte solutions. We observe that the current increases as a function of the applied external electric field  $E_x$  and as the cation valence increases. Therefore, at a given electric field different from zero,

the lowest current is produced in NaCl and the highest in LaCl<sub>3</sub>. Interestingly, the current is systematically higher in channels of conductors than in non-polarizable materials. At all the fields, we observe higher velocities in channels made of conductors than non-polarizable surfaces (for the velocity profiles, see Figure S4 in the Supporting Information). In addition, our data show that the current increases in a non-linear way. The non-linear behavior is enhanced in the slit-like pores made of conductors. The highest field applied in our simulations is 0.15 V/Å (1.5 × 10<sup>9</sup> V/m), higher than what real systems tolerate.<sup>38</sup> At the end of this section, we discuss how equivalent conditions may be created using weaker fields.



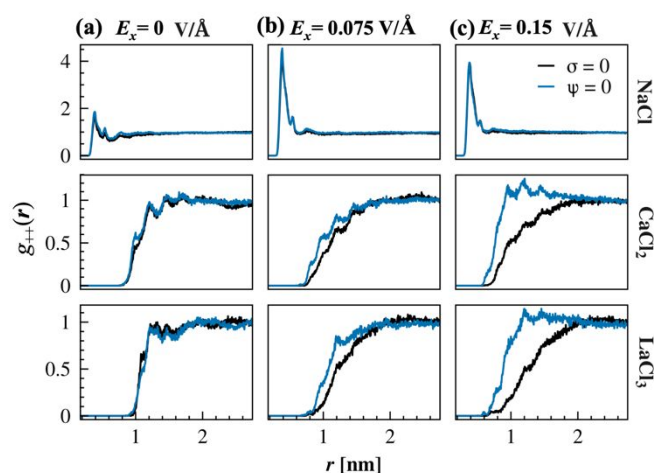
**Figure 5:** Ion transport in a slit-like nanochannel. Average current as a function of the applied external field  $E_x$  in electrolytes of (a) NaCl, (b) CaCl<sub>2</sub>, and (c) LaCl<sub>3</sub>. The electrolytes are confined between non-polarizable surfaces ( $\sigma = 0$ ) and conductors ( $\psi = 0$ ). The black lines represent the profiles in slit-like channels of conductors, while the light-blue lines are in non-polarizable surfaces. The separation distance between the surfaces is  $h = 0.97$  nm.

Figure 6 portrays the contributions to the total current from the two ionic components. In the systems confined by non-polarizable materials, the contribution to the current by both charge carriers, cations and anions, is approximately the same. Similarly, both ions contribute nearly equally to the current in the NaCl electrolyte confined by polarizable surfaces. However, there is a higher contribution from the cation in the CaCl<sub>2</sub> and LaCl<sub>3</sub> systems confined by polarizable surfaces. This phenomenon cannot be understood solely in terms of the higher ionic valence of the cations since it is not observed in non-polarizable systems. Therefore, it is an effect caused by the induced surface polarization.



**Figure 6:** Ionic current by components of (a) NaCl, (b) CaCl<sub>2</sub>, and (c) LaCl<sub>3</sub>. The top panels are correspond to slit channels made of non-polarizable ( $\sigma = 0$ ) surfaces whereas the bottom panels are for polarizable surfaces ( $\psi = 0$ ). Cations contribute to the ionic current

more than anions do at high fields and high ion valence. The separation distance between the surfaces is  $h = 0.97$  nm.



**Figure 7:** Cation-cation pair correlation functions  $g_{++}(r)$  in (a) NaCl, (b) CaCl<sub>2</sub>, and (c) LaCl<sub>3</sub> confined by slit channels made of non-polarizable ( $\sigma = 0$ ) and polarizable surfaces ( $\psi = 0$ ). Each row contains the profiles at external fields of  $E_x = 0, 0.075,$  and  $0.15$  V/Å. The black lines represent the profiles in slit-like channels of conductors, while the light-blue lines are in non-polarizable surfaces. The separation distance between the surfaces is  $h = 0.97$  nm.

We investigated the ionic density profiles as a function of the  $z$ -coordinate in the channel (see Figure S3 in the Supporting Information). We found that, in general, the cations tend to align at the channel center, whereas the anions are adsorbed on the walls. The ionic density profiles slightly change by applying an external field, but these changes are similar in channels made of conductors and non-polarizable surfaces. Therefore, the changes observed in the current cannot be explained in terms of the ionic distributions in the channel.

We look at the pair correlation functions to explain the enhance ionic transport in conductors. The pair correlation functions  $g_{+-}(r)$  and  $g_{-+}(r)$ , however, are similar in polarizable and non-polarizable systems (see Figures S5 and S6 in the Supporting Information). In Figure 7, the pair correlations functions between cations  $g_{++}(r)$  reveal that only monovalent cations approach other cations at all the fields  $E_x$ . The peaks' position implies that the clustering is mediated by the anions. At low fields, divalent and trivalent cations tend to be apart from other cations, however, the tendency to approach between cations increases at high fields in the polarizable systems (In Figure 7c, see  $g_{++}(r)$  at  $E_x = 0.15$  V/Å for CaCl<sub>2</sub> and LaCl<sub>3</sub>). Cations continue apart at high fields in the non-polarizable systems.

In terms of the pair correlation function, the potential of mean force between two ions is expressed as  $w_{ij}(r) = -k_B T \ln g_{ij}(r)$ . The mean force between the two ions is given as  $f(r) = -\frac{dw_{ij}(r)}{dr} = \frac{1}{g_{ij}(r)} \frac{dg_{ij}(r)}{dr}$ . Therefore, a negative slope of a pair correlation profile implies an attractive mean force between the ions. Figure 7 shows a region

(1 nm <  $r$  < 2 nm) where the slope of the  $g_{++}(r)$  profiles of divalent and trivalent cations between conductors is negative at the highest electric field. This implies an induced attractive force between the cations confined between conductors, whereas the cations confined between non-polarizable surfaces repel strongly. The attraction between the cations is a cooperative effect caused by the screening of the interactions by the conductors' polarization charge that reduces the repulsion between equally charged ions. The increased capability of cations to approach other cations when they are confined in polarizable surfaces allows them to transport the charge more efficiently.

We studied the ions' transport at surface potentials and charges different from zero. However, the ionic current does not change significantly with respect to the zero-charge and zero-potential conditions (see Figures S7 and S8 in the Supporting Information). This could result from the polarization charge fluctuations being unaffected at different applied fields and potentials.

Our study shows that changes in surface material induce a difference in ion transport properties at strong electric fields. However, the phenomena described here are difficult to observe in molecular simulations at electric fields lower than 0.05 V/Å because the dielectric response of water dominates. Effectively, the magnitude of the field experienced by any charge in the system  $|\mathbf{E}|$  is smaller than an external field  $|\mathbf{E}_{\text{ext}}|$ . The attenuation of the applied electric field is due to the induced polarization field that opposes the external field. Hence, the effective electric field is given as  $\mathbf{E} = \epsilon^{-1} \mathbf{E}_{\text{ext}}$ , where  $\epsilon$  is dielectric tensor, which has components  $\epsilon_{\parallel}$  and  $\epsilon_{\perp}$  greater than 1.

The polarization occurs via the water molecules' orientation and the ions' arrangement at timescales shorter than  $10^{-9}$  s. In water, a strong effective electric field  $\mathbf{E}$  may occur (even when  $\mathbf{E}_{\text{ext}}$  is not too strong) at a timescale faster than the system relaxation time when the components of  $\epsilon$  are still low. Such conditions can be created using a fast-oscillating AC external field. The effects observed here may also be relevant under weaker fields at lower temperatures or when the transport is induced by a combination of electric field and pressure gradients.

## Conclusions

We studied water and electrolyte solutions confined in nanometre-scale slit-like channels. By comparing slits made of conductors and non-polarizable surfaces, we showed that the surface polarization decreases the repulsion between equally charged ions and is further decreased for multivalent ions. The decreased repulsion between multivalent ions allows them to move collectively, leading to a more efficient ion transport. While confinement and the surface polarization charges induced in conductors affect the dielectric responses in the confined fluids, it is not enough to explain the increase of the ion conductivity by conductors. Nanochannels formed by

conductive electrodes are promising for designing highly efficient energy storage devices, ion removal processes, and bioinspired functions. Tunability of the ionic conduction and dielectric properties is desirable in some applications. Our results show that the conduction and the dielectric response of the confined liquid can be tuned by the dielectric and conductive properties of the confining surfaces.

Gaussian distribution of the polarization charge on the atoms of the conductors could serve to model the screening from electrons. For that, in the future, we will establish the relationship between the width of the Gaussian distribution ( $\kappa^{-1}$ ) and the electrons' screening correlation length ( $\lambda_{\text{TF}}$ ) from quantum mechanical calculations.

## Author Contributions

F. J.-A. and M. O. d. I. C. conceived the idea and designed the research. F. J.-A. and A. E. performed the simulations and the data analysis. The three authors contributed to the discussions and drafting of the manuscript.

## Conflicts of interest

There are no conflicts to declare.

## Acknowledgements

This work was funded by Award 70NANB19H005 from U.S. Department of Commerce, National Institute of Standards and Technology as part of the Center for Hierarchical Materials Design (CHiMaD) and by the Sherman Fairchild Foundation.

## References

- Schoch, R. B.; Han, J.; Renaud, P., Transport phenomena in nanofluidics. *Reviews of Modern Physics* **2008**, *80* (3), 839-883.
- Barrat, J.-L.; Bocquet, L., Large Slip Effect at a Nonwetting Fluid-Solid Interface. *Physical Review Letters* **1999**, *82* (23), 4671-4674.
- Buyukdagli, S., Nanofluidic Charge Transport under Strong Electrostatic Coupling Conditions. *The Journal of Physical Chemistry B* **2020**, *124* (49), 11299-11309.
- Geim, A. K.; Grigorieva, I. V., Van der Waals heterostructures. *Nature* **2013**, *499* (7459), 419-425.
- Fumagalli, L.; Esfandiari, A.; Fabregas, R.; Hu, S.; Ares, P.; Janardanan, A.; Yang, Q.; Radha, B.; Taniguchi, T.; Watanabe, K.; Gomila, G.; Novoselov, K. S.; Geim, A. K., Anomalously low dielectric constant of confined water. *Science* **2018**, *360* (6395), 1339-1342.
- Algara-Siller, G.; Lehtinen, O.; Wang, F. C.; Nair, R. R.; Kaiser, U.; Wu, H. A.; Geim, A. K.; Grigorieva, I. V., Square ice in graphene nanocapillaries. *Nature* **2015**, *519* (7544), 443-445.
- Han, S.; Choi, M. Y.; Kumar, P.; Stanley, H. E., Phase transitions in confined water nanofilms. *Nature Physics* **2010**, *6* (9), 685-689.
- Giovambattista, N.; Rossky, P. J.; Debenedetti, P. G., Phase Transitions Induced by Nanoconfinement in Liquid Water. *Physical Review Letters* **2009**, *102* (5), 050603.

9. Mouterde, T.; Keerthi, A.; Poggioli, A. R.; Dar, S. A.; Siria, A.; Geim, A. K.; Bocquet, L.; Radha, B., Molecular streaming and its voltage control in ångström-scale channels. *Nature* **2019**, *567* (7746), 87-90.
10. Krishnan, K. S.; Ganguli, N., Large Anisotropy of the Electrical Conductivity of Graphite. *Nature* **1939**, *144* (3650), 667-667.
11. Wang, J.; Ma, F.; Sun, M., Graphene, hexagonal boron nitride, and their heterostructures: properties and applications. *RSC Advances* **2017**, *7* (27), 16801-16822.
12. Bessler, R.; Duerig, U.; Koren, E., The dielectric constant of a bilayer graphene interface. *Nanoscale Advances* **2019**, *1* (5), 1702-1706.
13. Siepmann, J. I.; Sprik, M., Influence of surface topology and electrostatic potential on water/electrode systems. *The Journal of Chemical Physics* **1995**, *102* (1), 511-524.
14. Reed, S. K.; Lanning, O. J.; Madden, P. A., Electrochemical interface between an ionic liquid and a model metallic electrode. *The Journal of Chemical Physics* **2007**, *126* (8), 084704.
15. Jadhao, V.; Solis, F. J.; de la Cruz, M. O., Simulation of Charged Systems in Heterogeneous Dielectric Media via a True Energy Functional. *Physical Review Letters* **2012**, *109* (22), 223905.
16. Jadhao, V.; Solis, F. J.; Cruz, M. O. d. I., A variational formulation of electrostatics in a medium with spatially varying dielectric permittivity. *The Journal of Chemical Physics* **2013**, *138* (5), 054119.
17. Torrie, G. M.; Valleau, J. P.; Patey, G. N., Electrical double layers. II. Monte Carlo and HNC studies of image effects. *The Journal of Chemical Physics* **1982**, *76* (9), 4615-4622.
18. Messina, R., Image charges in spherical geometry: Application to colloidal systems. *The Journal of Chemical Physics* **2002**, *117* (24), 11062-11074.
19. Son, C. Y.; Wang, Z.-G., Image-charge effects on ion adsorption near aqueous interfaces. *Proceedings of the National Academy of Sciences* **2021**, *118* (19), e2020615118.
20. Nguyen, T. D.; Li, H.; Bagchi, D.; Solis, F. J.; Olvera de la Cruz, M., Incorporating surface polarization effects into large-scale coarse-grained Molecular Dynamics simulation. *Computer Physics Communications* **2019**, *241*, 80-91.
21. Ahrens-Iwers, L. J. V.; Meißner, R. H., Constant potential simulations on a mesh. *The Journal of Chemical Physics* **2021**, *155* (10), 104104.
22. Scalfi, L.; Limmer, D. T.; Coretti, A.; Bonella, S.; Madden, P. A.; Salanne, M.; Rotenberg, B., Charge fluctuations from molecular simulations in the constant-potential ensemble. *Physical Chemistry Chemical Physics* **2020**, *22* (19), 10480-10489.
23. Santos, A. P. d.; Giroto, M.; Levin, Y., Simulations of Coulomb systems confined by polarizable surfaces using periodic Green functions. *The Journal of Chemical Physics* **2017**, *147* (18), 184105.
24. Lamoureux, G.; Roux, B. t., Modeling induced polarization with classical Drude oscillators: Theory and molecular dynamics simulation algorithm. *The Journal of Chemical Physics* **2003**, *119* (6), 3025-3039.
25. Comtet, J.; Niguès, A.; Kaiser, V.; Coasne, B.; Bocquet, L.; Siria, A., Nanoscale capillary freezing of ionic liquids confined between metallic interfaces and the role of electronic screening. *Nature Materials* **2017**, *16* (6), 634-639.
26. Schlaich, A.; Jin, D.; Bocquet, L.; Coasne, B., Electronic screening using a virtual Thomas–Fermi fluid for predicting wetting and phase transitions of ionic liquids at metal surfaces. *Nature Materials* **2022**, *21* (2), 237-245.
27. Ashcroft, N. W.; Mermin, N. D., *Solid state physics*. Cengage Learning: 2022.
28. Lieb, E. H.; Simon, B., Thomas-Fermi Theory Revisited. *Physical Review Letters* **1973**, *31* (11), 681-683.
29. Jiménez-Ángeles, F.; Harmon, K. J.; Nguyen, T. D.; Fenter, P.; Olvera de la Cruz, M., Nonreciprocal interactions induced by water in confinement. *Physical Review Research* **2020**, *2* (4), 043244.
30. Yeh, I.-C.; Berkowitz, M. L., Ewald summation for systems with slab geometry. *The Journal of Chemical Physics* **1999**, *111* (7), 3155-3162.
31. Berendsen, H. J. C.; Grigera, J. R.; Straatsma, T. P., The missing term in effective pair potentials. *The Journal of Physical Chemistry* **1987**, *91* (24), 6269-6271.
32. Jorgensen, W. L.; Maxwell, D. S.; Tirado-Rives, J., Development and Testing of the OPLS All-Atom Force Field on Conformational Energetics and Properties of Organic Liquids. *Journal of the American Chemical Society* **1996**, *118* (45), 11225-11236.
33. Thompson, A. P.; Aktulga, H. M.; Berger, R.; Bolintineanu, D. S.; Brown, W. M.; Crozier, P. S.; in 't Veld, P. J.; Kohlmeyer, A.; Moore, S. G.; Nguyen, T. D.; Shan, R.; Stevens, M. J.; Tranchida, J.; Trott, C.; Plimpton, S. J., LAMMPS - a flexible simulation tool for particle-based materials modeling at the atomic, meso, and continuum scales. *Computer Physics Communications* **2022**, *271*, 108171.
34. Xue, J.; Sanchez-Yamagishi, J.; Bulmash, D.; Jacquod, P.; Deshpande, A.; Watanabe, K.; Taniguchi, T.; Jarillo-Herrero, P.; LeRoy, B. J., Scanning tunnelling microscopy and spectroscopy of ultra-flat graphene on hexagonal boron nitride. *Nature Materials* **2011**, *10* (4), 282-285.
35. Bonthuis, D. J.; Gekle, S.; Netz, R. R., Dielectric Profile of Interfacial Water and its Effect on Double-Layer Capacitance. *Physical Review Letters* **2011**, *107* (16), 166102.
36. Ballenegger, V.; Hansen, J.-P., Dielectric permittivity profiles of confined polar fluids. *The Journal of Chemical Physics* **2005**, *122* (11), 114711.
37. Zhang, C.; Gygi, F.; Galli, G., Strongly Anisotropic Dielectric Relaxation of Water at the Nanoscale. *The Journal of Physical Chemistry Letters* **2013**, *4* (15), 2477-2481.
38. Hogg, M. G.; Timoshkin, I. V.; Given, M. J.; Wilson, M. P.; Macgregor, S. J.; Wang, T.; Fouracre, R. A.; Lehr, J. M., Impulse breakdown of water with different conductivities. *IEEE Transactions on Dielectrics and Electrical Insulation* **2012**, *19* (5), 1559-1568.